

Gap structure of the non-symmorphic superconductor LaNiGa₂ probed by μ SR

Shyam Sundar¹, M. Yakovlev², N. Azari², M. Abedi², D. M. Broun², H. U. Özdemir², S. R. Dunsiger^{2,3}, D. Zackaria⁴, V. Taufour⁴ and J. E. Sonier²

¹*Scottish Universities Physics Alliance, School of Physics and Astronomy,
University of St. Andrews, KY16 9SS, United Kingdom*

²*Department of Physics, Simon Fraser University, Burnaby, British Columbia V5A 1S6, Canada*

³*Centre for Molecular and Materials Science, TRIUMF, Vancouver, British Columbia V6T 2A3, Canada*

⁴*Department of Physics and Astronomy, University of California, Davis, California 95616, USA*

(Dated: November 2, 2023)

We report muon spin rotation (μ SR) measurements of the temperature dependence of the absolute value of the magnetic penetration depth and the magnetic field dependence of the vortex core size in the mixed state of the non-symmorphic superconductor LaNiGa₂. The temperature dependence of the normalized superfluid density is shown to be well described by a two-band model with strong interband coupling. Consistent with a strong coupling of the superconducting condensates in two different bands, we show that the field dependence of the vortex core size resembles that of a single-band superconductor. Our results lend support to the proposal that LaNiGa₂ is a fully-gapped, internally antisymmetric nonunitary spin-triplet superconductor.

I. INTRODUCTION

Superconductors exhibiting nontrivial topology have garnered significant attention in the field of condensed matter physics. Of particular interest is the prediction that topological superconductors can host Majorana zero modes, which may be used as building blocks for a quantum computer robust to environmental noise [1, 2]. Recently, LaNiGa₂ has been identified as a potential topological superconductor via an investigation of newly synthesized high-quality single crystals [3]. The enhanced quality of the single crystals compared to previously studied polycrystalline samples has revealed a topological electronic band structure arising from non-symmorphic symmetries in the centrosymmetric space group of LaNiGa₂. In addition to the topological character, LaNiGa₂ is believed to have an unconventional superconducting order parameter that breaks time-reversal symmetry (TRS). Zero-field μ SR measurements on polycrystalline LaNiGa₂ have detected the onset of weak spontaneous internal magnetic fields at the superconducting transition temperature (T_c), which is a signature of a TRS breaking superconductor [4]. In addition, two nodeless superconducting gaps have been inferred from measurements of the temperature dependences of the specific heat, upper critical field and magnetic penetration depth (by a tunnel diode oscillator method) in polycrystalline LaNiGa₂ [5]. The occurrence of a nodeless two-gap superconducting state that breaks TRS has been explained by an internally antisymmetric nonunitary triplet (INT) state in which there is both spin-up ($\uparrow\uparrow$) and spin-down ($\downarrow\downarrow$) pairing between electrons on two different atomic orbitals [5–7].

The INT state has also been invoked to account for fully-gapped TRS breaking in the compositionally related noncentrosymmetric superconductor LaNiC₂. Evidence for a broken TRS superconducting state in LaNiC₂ has also been observed by zero-field μ SR in both polycrystalline [8] and single-crystal [9] samples. Although

different experiments have yielded inconsistent conclusions on the nature of the superconducting gap structure of LaNiC₂ [10–16], the existence of two nodeless superconducting gaps was recently unambiguously verified by transverse-field (TF) μ SR measurements of the low-field magnetic penetration depth and low-temperature vortex core size in the mixed state of single crystals [9]. The two nodeless gaps manifest as a simultaneous crossover in the field dependences of an effective magnetic penetration depth and the vortex core size due to delocalization of the quasiparticle vortex-core states associated with the smaller gap.

In stark contrast to the high-quality single crystals of LaNiGa₂ in which topological superconductivity has recently been recognized [3], the electronic specific heat of the polycrystalline LaNiGa₂ sample investigated in Ref. [5] exhibits a rather broad superconducting transition that is suggestive of significant inhomogeneity. The shape of the broad transition and its evolution with applied magnetic field is potentially an indication of a double phase transition. This raises the possibility of nearly degenerate unconventional pairing states with critical temperatures that are split by non-magnetic disorder. Since disorder can alter the temperature dependence of the physical quantities previously measured in polycrystalline LaNiGa₂, further evidence of there being two nodeless superconducting gaps is needed.

Here we report on a TF- μ SR investigation of the superconducting energy-gap structure in LaNiGa₂ single crystals that exhibit a sharp single superconducting transition in the temperature dependence of the specific heat. From measurements that probe the magnetic field distribution in the vortex (mixed) state, we find that the temperature dependence of the normalized superfluid density for a magnetic field applied parallel to the b -axis is consistent with two nodeless superconducting energy gaps having magnitudes close to the sizes of the two apparent gaps in LaNiC₂. In contrast to LaNiC₂, however, this data for LaNiGa₂ indicates strong interband coupling.

This is substantiated by the magnetic field dependence of the vortex core size, which as expected for strong coupling between two different band condensates, resembles that of a single isotropic gap superconductor in the clean limit.

II. EXPERIMENTAL DETAILS

Single crystals of LaNiGa_2 were grown using a Ga deficient self-flux technique, as described in Ref. [3]. Bulk superconductivity in the single crystals is observed at $T_c = 1.96$ K. The TF- μ SR experiments were performed on the M15 surface muon beamline at TRIUMF, utilizing a top-loading dilution refrigerator. The sample consisted of multiple b -axis aligned LaNiGa_2 single crystals arranged in a mosaic and mounted onto a pure Ag plate of dimensions $12.5 \text{ mm} \times 22 \text{ mm} \times 0.25 \text{ mm}$, as shown in the inset of Fig. 1(b). The crystals covered $\sim 70\%$ of the Ag plate. To minimize the contribution to the TF- μ SR signal from muons stopping outside the sample, three thin wafers of intrinsic GaAs were used to cover the exposed end of the Ag backing plate. We note that GaAs does not produce any detectable muon precession signal within the field range considered in our study. The external magnetic field was applied parallel to the b axis of the LaNiGa_2 single crystals and perpendicular to the initial muon-spin polarization $\mathbf{P}(t=0)$. The magnetic field was applied above T_c and the sample subsequently cooled down to the desired temperature in the superconducting state. The magnetic field distribution in the vortex state was probed for each temperature and magnetic field by measuring the time evolution of the muon-spin polarization via detection of the decay positrons from an implanted ensemble of ~ 15 million positive muons. Further details on the TF- μ SR method utilized in this study may be found in Ref. [17].

III. DATA ANALYSIS AND RESULTS

Figure 1(a) displays representative TF- μ SR asymmetry spectra recorded in the normal and superconducting states of LaNiGa_2 for an applied magnetic field of $H = 408$ Oe. The weak damping of the TF- μ SR asymmetry spectrum in the normal state at $T = 2.5$ K is due to the magnetic field distribution associated with nuclear dipole moments sensed by muons that stopped in the sample and the exposed area of the Ag backing plate. The larger depolarization rate of the TF- μ SR signal at 0.096 K is a result of muons randomly sampling the spatial distribution of magnetic field generated by the vortex lattice below T_c . Figure 1(b) shows Gaussian-apodized Fourier transforms of the TF- μ SR signals. The Fourier transforms are an approximate visual representation of the magnetic field distribution detected by the muons inside and outside the sample, because of the additional broadening by the apodization used to remove the ring-

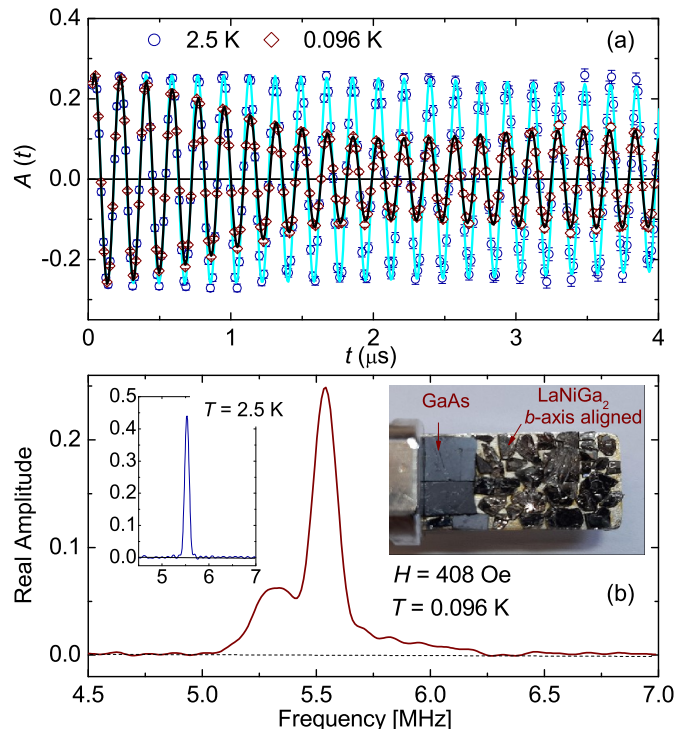


FIG. 1. (a) TF- μ SR asymmetry spectra measured above and below T_c for a magnetic field of $H = 408$ Oe. The oscillating lines through the data points represent fits to Eqs. (1) and (2) for temperatures above and below T_c , respectively. (b) Fourier transform of the TF- μ SR signal for $T = 0.096$ K. The large peak at 5.53 MHz is a result of muons stopping outside the sample. Left inset: Fourier transform of the TF- μ SR signal for $T = 2.5$ K. Right inset: Photograph showing the LaNiGa_2 single crystals and GaAs wafers attached to the Ag backing plate, which is anchored to the Ag sample holder of the dilution refrigerator. The single crystals are mounted with their b axis aligned in the direction of the applied magnetic field, which is perpendicular to the plane of the Ag backing plate.

ing and noise associated with the finite time range and reduced number of muon decay events at later times [17]. Below T_c , the Fourier transform displays a distinct peak at the frequency corresponding to the applied field associated with muons that missed the sample and stopped in the Ag backing plate. This background peak is superimposed on an asymmetric lineshape that comes from muons that sensed the spatial distribution of field of the vortex lattice and the nuclear moments in the LaNiGa_2 single crystals.

Above T_c , the TF- μ SR asymmetry spectrum is well described by the sum of two Gaussian damped cosine functions

$$A(t) = a_s e^{\sigma_s^2 t^2} \cos(2\pi\nu_s t + \phi) + a_{bg} e^{\sigma_{bg}^2 t^2} \cos(2\pi\nu_{bg} t + \phi). \quad (1)$$

The first term describes the signal from muons that stop in the LaNiGa_2 single crystals, while the second

term accounts for the signal coming from muons stopping outside the sample. The precession frequencies ν_i ($i = s, \text{bg}$) are a measure of the corresponding mean local field $B_i = 2\pi\nu_i/\gamma_\mu$ sensed by the muons, where $\gamma_\mu/2\pi = 13.5539$ MHz/kG is the muon gyromagnetic ratio. The parameter ϕ is the initial phase of the muon spin polarization relative to the positron counters, which depends on the degree of Larmor precession of the muon spin in the applied field before reaching the sample.

The TF- μ SR signals below T_c are well fit assuming the following modified analytical Ginzburg-Landau (GL) model [18] for the spatial variation of the internal magnetic field generated by the vortex lattice with supercurrents flowing in the ij ($=ac$) plane

$$B(\mathbf{r}) = \sum_{\mathbf{G}} \frac{B_0(1-b^4)e^{-i\mathbf{G}\cdot\mathbf{r}} u K_1(u)}{\lambda_{ij}^2 G^2 + \lambda_{ij}^4 (n_{xxyy} G^4 + d G_x^2 G_y^2)}. \quad (2)$$

Here $b = B/B_{c2}$ is the reduced field (where $B_{c2} = \Phi_0/2\pi\xi_{ij}^2$ is the upper critical magnetic field for a field applied perpendicular to the ij plane), B_0 is the average internal magnetic field, \mathbf{G} are the reciprocal lattice vectors of the vortex lattice, $u^2 = 2\xi_{ac}^2 G^2(1+b^4)[1-2b(1-b)^2]$, $K_1(u)$ is a modified Bessel function, n_{xxyy} and d are dimensionless parameters arising from nonlocal corrections, and λ_{ij} and ξ_{ij} are the GL magnetic penetration depth and coherence length. Equation (2) accounts for potential changes in the vortex lattice geometry, ranging from hexagonal to square. The fits of the TF- μ SR asymmetry spectra below T_c were done by replacing the sample term in Eq. (1) with

$$A_s(t) = a_s \exp [(\sigma_n^2 + \sigma_{\text{dis}}^2)t^2] \sum_{\mathbf{r}} \cos [\gamma_\mu B(\mathbf{r})t + \phi], \quad (3)$$

where $B(\mathbf{r})$ is given by Eq. (2). The depolarization rate σ_n is the value of σ_s above T_c , which is due to the nuclear dipoles in the sample and is independent of temperature. The sum is over real-space positions in an ideal periodic vortex lattice, while the depolarization rate σ_{dis} accounts for further broadening of the internal magnetic field distribution by frozen disorder in the vortex lattice. Based on previous μ SR studies of type-II superconductors [19], we assumed σ_{dis} is proportional to $1/\lambda_{ac}^2$.

Good fits to TF- μ SR spectra recorded for an applied field of $H = 150$ Oe were achieved for all temperatures below T_c assuming an hexagonal vortex lattice, with $n_{xxyy} = 0$ and $d = 0$. The same is true for TF- μ SR spectra recorded for $H \leq 400$ Oe and $T = 0.096$ K. However, for $H = 800$ Oe and $T = 0.096$ K, a good fit could not be achieved with the assumption of an hexagonal vortex lattice. Instead, a good quality fit was achieved by lifting this constraint, yielding $n = (4.5 \pm 8.7) \times 10^{-8}$, $d = 0.29 \pm 0.18$, and $\beta = 90 \pm 17^\circ$, where β is the acute angle of the rhombic unit cell of the vortex lattice. Even without assuming the vortex lattice structure, we could not achieve a good fit of an additional TF- μ SR asymmetry spectrum recorded for $H = 600$ Oe and $T = 0.096$ K. This

is perhaps due to a superposition of distorted hexagonal and square vortex lattices between the field-induced hexagonal-to-square lattice transition. In all likelihood the vortex-lattice transition is driven by the anisotropy of the Fermi surface [20] in the ac plane, which is close to having four-fold symmetry [3].

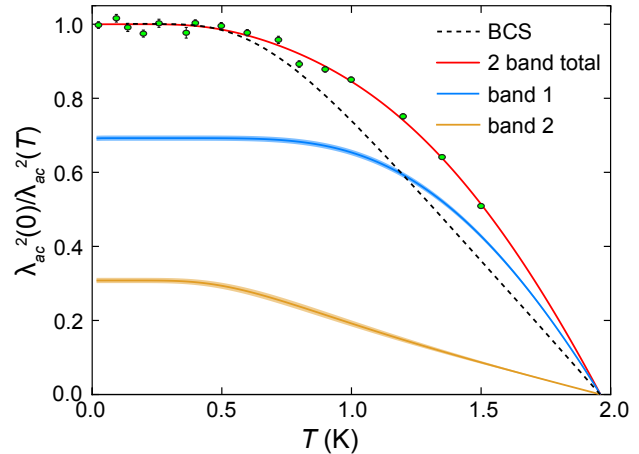


FIG. 2. Temperature dependence of the normalized superfluid density, $\lambda_{ac}^2(0)/\lambda_{ac}^2(T)$, in LaNiGa₂ for $H = 150$ Oe. Circles denote μ SR data points and error bars give the standard error at each temperature. Dashed curve is the normalized superfluid density from single-band BCS theory [21]. Upper solid curve is the total normalized superfluid density in the two-band model for the density of states parameter $n_1 = 0.8$, with contributions from the individual bands shown below it. Shaded areas denote the $1\text{-}\sigma$ uncertainty regions associated with the model fit. Fit parameters are given in the Appendix.

As one of few techniques able to reliably probe the *absolute value* of the magnetic penetration depth, μ SR correctly obtains the shape of the superfluid density $\rho_s(T)$. We can then infer information about the magnitude, anisotropy and temperature dependence of the energy gap, and the strength and nature of the pairing interaction, by fitting generalized Bardeen-Cooper-Schrieffer (BCS) models to the superfluid density. For LaNiGa₂, the normalized low-field superfluid density, $\lambda_{ac}^2(0)/\lambda_{ac}^2(T)$, where $\lambda_{ac}(0) = 1510 \pm 4$ Å, is shown in Fig. 2. We can immediately see from Fig. 2 that the superfluid density in LaNiGa₂ is distinctly different from that of a single-band BCS superconductor, in particular having larger magnitude in the upper half of the superconducting temperature range. We will later see that this is the experimental signature of strong interband pairing. The value of $\lambda_{ac}(0)$ is much smaller than the μ SR-determined value of the effective magnetic penetration depth $\lambda(0) = 3500 \pm 100$ Å in a polycrystalline LaNiGa₂ sample [4]. For polycrystalline samples, the internal magnetic field distribution measured by μ SR in the vortex state is an average over all orientations of the external magnetic field with respect to the crystalline axes. Consequently, $\lambda(0)$ is an average of the a -axis, b -axis and c -axis magnetic penetration depths, which have

been estimated to be $\lambda_a = 1740 \text{ \AA}$, $\lambda_b = 5090 \text{ \AA}$ and $\lambda_c = 1890 \text{ \AA}$ from a combination of thermodynamic critical field $H_c(T)$ and anisotropic upper critical field $H_{c2}(T)$ data from measurements on LaNiGa₂ single crystals [3]. For a single crystal with the field applied parallel to the b -axis, we expect our μ SR determined value of $\lambda_{ac}(0)$ to be closer to the effective penetration depth $\sqrt{\lambda_a \lambda_c} = 1813 \text{ \AA}$ calculated using these approximate values of λ_a and λ_c .

To capture the behavior of the superfluid density, we turn to a two-band BCS model, which can be viewed as the low energy effective theory of a superconductor displaying significant anisotropy of pairing over the Fermi surface, but without nodal lines or point nodes in the energy gap. The two-band model we use has been presented in detail in Ref. [22] and has been successfully used to describe the superconductivity in the non-centrosymmetric material LaNiC₂ (Ref. [9]), although we note from the outset that the inferences drawn about the pairing interactions in LaNiGa₂ are quite different from those in LaNiC₂, likely reflecting the different symmetry-allowed superconducting order parameters in the two materials.

In a nutshell, the two-band model partitions the Fermi surface into two disparate pieces, and allows for pairing interactions within (intraband) and between (interband) the two subsystems. When the gap equation is solved for such a system, as described in the Appendix, we generically find two distinct energy gaps, of different magnitude. BCS-type superconductivity is characterized by thermally activated behavior in low temperature properties such as the superfluid density. Accordingly, the leading low-temperature behavior of the superfluid density (*i.e.*, the temperature range over which significant T dependence develops) is set by the magnitude of the subdominant gap. This is particularly apparent in the lower, band-2 curve in the decomposition of $\lambda_{ac}^2(0)/\lambda_{ac}^2(T)$ in Fig. 2. From this we obtain a gap ratio of $\Delta_2(0)/k_B T_c = 1.23$ for the subdominant band. In the two-band model, the magnitude of the dominant gap is set by T_c itself, leading to $\Delta_1(0)/k_B T_c = 2.62$ for LaNiGa₂. This is much larger than the BCS gap ratio of 1.76, and indicates a tension between the pairing in the two bands, with the intraband pairing being intrinsically repulsive in band 2. We note that the gap ratios are comparable to the values 1.29 and 2.04 deduced from superfluid density measurements of polycrystalline LaNiGa₂ in Ref. [5].

As we can see in Fig. 2, the two-band model provides an excellent fit to the normalized superfluid density, and is readily able to capture the enhancement of $\lambda_{ac}^2(0)/\lambda_{ac}^2(T)$ in the upper half of the temperature range. One of the robust conclusions to emerge from the two-band analysis, which is summarized in Table 1 of the Appendix, is the existence of a very significant interband contribution to the pairing, something that has been proposed [5, 7] as being expected for the unusual type of superconductivity thought to exist in LaNiGa₂.

Figure 3 shows the dependence of λ_{ac} and ξ_{ac} on the

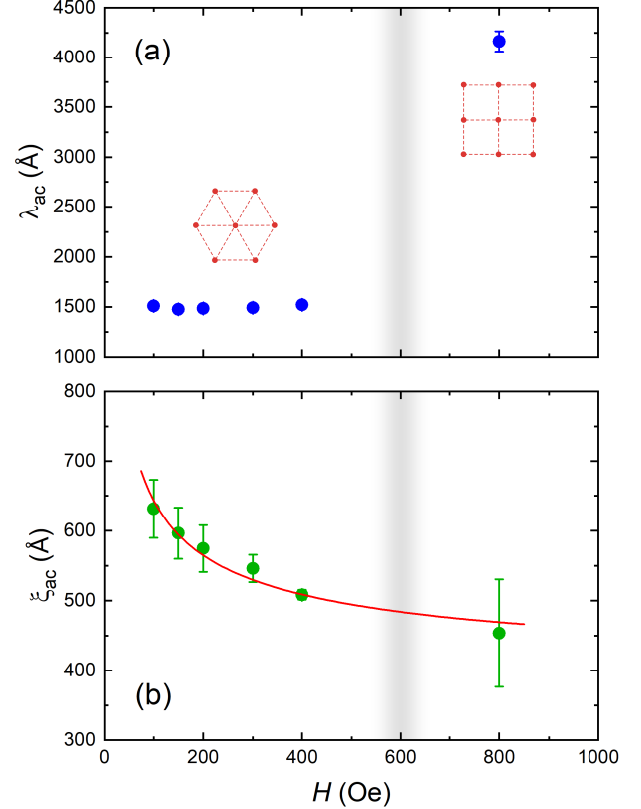


FIG. 3. (a) Magnetic field dependence of λ_{ac} in LaNiGa₂ for $T = 0.096 \text{ K}$ from fits indicating hexagonal and square vortex lattices for $H \leq 400 \text{ Oe}$ and $H = 800 \text{ Oe}$, respectively. (b) Magnetic field dependence of ξ_{ac} in LaNiGa₂. The solid curve through the data points is a fit to $\xi_{ac} = a + b/\sqrt{H}$, where $a = 374 \pm 19 \text{ \AA}$ and $b = 2704 \pm 269 \text{ \AA} \cdot \text{Oe}^{1/2}$.

applied magnetic field for $T = 0.096 \text{ K}$. Below $H = 400 \text{ Oe}$, which corresponds to the reduced field $b \sim 0.4$, λ_{ac} is independent of the applied field. This is in stark contrast to the rapid increase in λ_{ij} ($ij = ab, bc$ or ac) with increasing field at low b determined by μ SR in superconductors with gap nodes [19, 23] or strong gap anisotropy [24, 25]. A strong H dependence of λ_{ij} determined by μ SR may also occur at low b in weakly-coupled two-band superconductors, due to a faster suppression of the contribution from the weaker small-gap band to the superfluid density [26–28].

In general, an increase in the μ SR-determined value of λ_{ij} with increasing magnetic field does not necessarily imply a field-induced change in the superfluid density, but may instead reflect a failure of the assumed model for $B(\mathbf{r})$ to adequately describe changes in the decay of magnetic field around a vortex as the overlap between vortices increases [19]. We also note that not all μ SR studies assume a theoretical model for $B(\mathbf{r})$. A strong decrease in the square root of the second moment of the local magnetic field distribution measured by μ SR in the

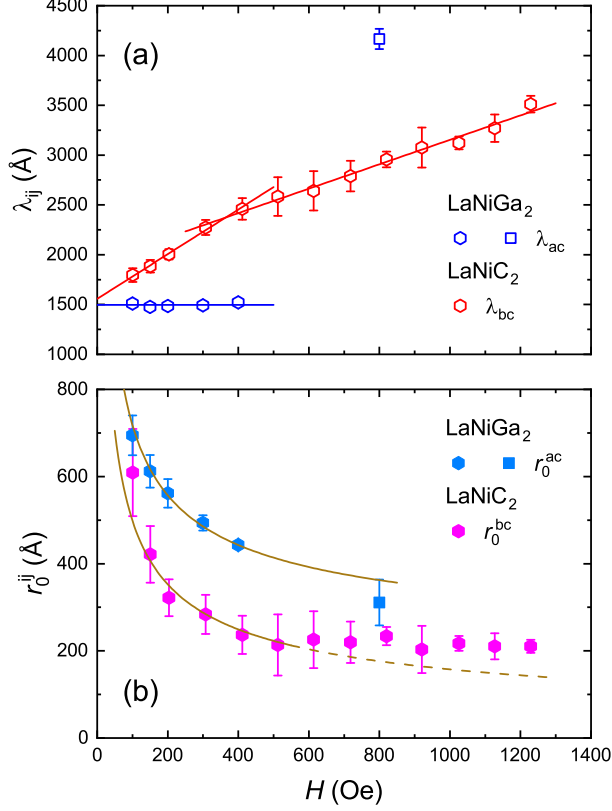


FIG. 4. Comparison of the magnetic field dependences of the fitted values of (a) λ_{ac} and (b) ξ_{ac} in LaNiGa₂ for $T = 0.096$ K and $\mathbf{H} \parallel \mathbf{b}$ with the values of λ_{bc} and ξ_{bc} in LaNiC₂ for $T = 0.05$ K and $\mathbf{H} \parallel \mathbf{a}$ from Ref. [9]. The solid lines through the data point in (a) are guides to the eye. The curves through the data points in (b) are fits to $r_0^{ij} = a + b/\sqrt{H}$, where $a = 168(28)$ Å and $b = 5504(452)$ Å·Oe^{1/2} for the core size r_0^{ac} in LaNiGa₂. The fit to the field dependence of the core size r_0^{bc} for LaNiC₂ is to the data at $H \leq 400$ Oe, where $a = 0$ Å and $b = 4986(228)$ Å·Oe^{1/2}. The hexagonal and square data symbols for LaNiGa₂ indicate the geometrical arrangement of the vortices.

vortex state of various superconductors has been interpreted in terms of a field-induced reduction of the superfluid density or increase in the “true” magnetic penetration depth [29–32]. Nevertheless, the H -independent behavior of λ_{ac} in Fig. 3(a) up to $H = 400$ Oe indicates that the field does not induce a change in the superfluid density below $b \sim 0.4$.

The absence of any change in λ_{ac} for LaNiGa₂ below $b \sim 0.4$ rules out the presence of gap nodes and is in stark contrast to the strong field dependence of λ_{bc} in the noncentrosymmetric superconductor LaNiC₂ [9] [see Fig. 4(a)]. In LaNiC₂, λ_{bc} exhibits an H -linear dependence with a slope change above $b \sim 0.2$, which is indicative of two superconducting gaps. By contrast, the field dependence of λ_{ac} in LaNiGa₂ closely resem-

bles the behavior of the effective magnetic penetration depth measured by μ SR in V₃Si, which also exhibits an hexagonal-to-square vortex lattice transition accompanied by a change in the fitted value of λ_{ij} [18]. Recent experiments suggest V₃Si has two distinct nodeless superconducting gaps [33, 34]. Consequently, the constant value of λ_{ac} below $b \sim 0.4$ for LaNiGa₂ does not rule out the occurrence of two gaps.

Less ambiguous is the meaning of the field dependence of ξ_{ac} shown in Fig. 3(b), which except at low H , more or less tracks the dependence of the vortex core size on magnetic field [19]. The vortex core size (r_0) is accurately determined by calculating the absolute value of the supercurrent density profile $|j(\mathbf{r})|$ from the experimental $B(\mathbf{r})$ and defining r_0 to be the distance from the core center along the nearest-neighbor vortex direction to the peak in $|j(\mathbf{r})|$ [35]. It has been shown that the field dependence of r_0 measured by μ SR precisely accounts for the field dependence of the electronic thermal conductivity measured in V₃Si, 2H-NbSe₂ and LuNi₂B₂C [19]. The physical picture is that the vortex core size shrinks with increasing magnetic field as a result of an increased intervortex transfer of quasiparticles at higher fields, where the distance between vortices is smaller [36, 37]. The increased delocalization of the bound quasiparticle vortex core states is detected in the electronic thermal conductivity measurements [38]. As can be seen in Figs 3(b) and 4(b), the field dependences of ξ_{ac} and the vortex core size r_0^{ac} for LaNiGa₂ are approximately described by an expression of the form $a + b/\sqrt{H}$, which is the predicted behavior of the vortex core size in clean isotropic-gapped BCS superconductors [39]. This is distinct from the two-band behavior of the vortex core size in LaNiC₂ [see Fig. 4(b)] and that reported earlier for 2H-NbSe₂ [26], where the core size rapidly decreases with increasing field and becomes independent of H at higher fields — although admittedly there is insufficient data for LaNiGa₂ at higher field (because of the field-induced vortex-lattice transition) to completely rule out a crossover to H -independent behavior.

The gap values determined from the analysis of the data in Fig. 2 ($\Delta_1 = 0.44$ meV and $\Delta_2 = 0.21$ meV) are comparable to the size of the two gaps in LaNiC₂ ($\Delta_1 = 0.42$ meV and $\Delta_1 = 0.18$ meV) determined in Ref. [9]. Hence, the different field dependences of λ_{ij} and r_0^{ij} exhibited by LaNiGa₂ and LaNiC₂ in Figs. 4(a) and 4(b) are not due to dissimilar sizes of the two gaps. Interestingly, the low-temperature $H \rightarrow 0$ extrapolated value of λ_{ac} for LaNiGa₂ is close to the low-temperature $H \rightarrow 0$ extrapolated value of λ_{bc} for LaNiC₂, and the low-temperature, low-field values of r_0^{ac} for LaNiGa₂ and r_0^{bc} for LaNiC₂ are also comparable. It is possible that with increasing field a significant anisotropy develops for the ratios $\lambda_{ac}/\lambda_{bc}$ and r_0^{ac}/r_0^{bc} , due to two-gap or anisotropic single-gap superconductivity. However, the H -independent behavior exhibited by λ_{ac} in LaNiGa₂ for $H \leq 400$ Oe suggests that this is unlikely to be the origin of the different field dependences of λ_{ij} and r_0^{ij} for the

two compounds displayed in Figs. 4(a) and 4(b).

The different field dependences of these parameters for the two compounds has a different origin. Theoretically, it has been shown that in two-band *s*-wave superconductors with a significant difference in the magnitudes of the two gaps, the spatial variation of the superconducting order parameter near the vortex core is the same in both bands when there is strong interband coupling [40, 41]. Consequently, the magnetic field dependence of the vortex-core size in the different bands is the same and resembles that of a single-band superconductor. Thus the single-gap like field dependences of λ_{ac} and r_0^{ac} for LaNiGa₂ may be attributed to the strong interband coupling deduced from the analysis of the temperature dependence of the normalized superfluid density.

To summarize, we have used μ SR to investigate the temperature dependence of the superfluid density and magnetic field dependence of the vortex core size in LaNiGa₂ single crystals. Together they are explained by two-band nodeless gap superconductivity with strong interband coupling. This lends support to the applicability of the proposed INT pairing state [5–7] to superconductivity in LaNiGa₂, which attributes the occurrence of the two gaps to the two spin-triplet states, $\uparrow\uparrow$ and $\downarrow\downarrow$, associated with Cooper pairing of electrons on two different Ni orbitals. The strong interband pairing inferred from our experimental results is notably inherent in the INT state.

IV. APPENDIX: TWO-BAND SUPERCONDUCTIVITY

A. Two-band BCS theory

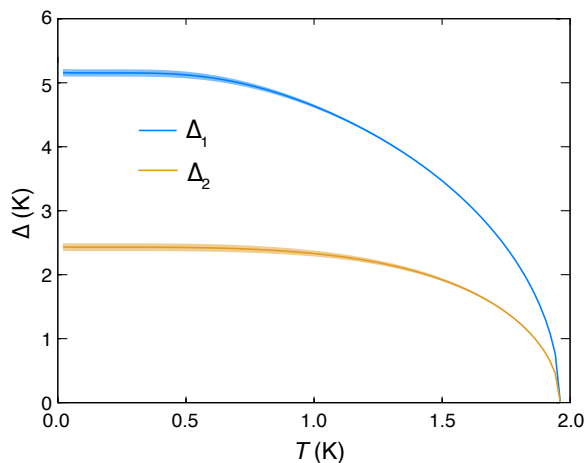


FIG. 5. Temperature dependence of the energy gaps, Δ_1 and Δ_2 , for LaNiGa₂ in the two-band model, for DOS parameter $n_1 = 0.8$. Shaded areas denote the $1\text{-}\sigma$ uncertainty regions associated with the model fit. The zero-temperature gap ratios, $\Delta(0)_i/k_B T_c$, are 2.62 and 1.23, respectively.

In the Matsubara formalism, the temperature dependent gap equation for a weak-coupling superconductor is

$$\Delta_{\mathbf{k}} = 2\pi T N_0 \sum_{\omega_n > 0}^{\omega_0} \left\langle V_{\mathbf{k}, \mathbf{k}'} \frac{\Delta_{\mathbf{k}'}}{\sqrt{\Delta_{\mathbf{k}'}^2 + \hbar^2 \omega_n^2}} \right\rangle_{\text{FS}} \quad (4)$$

where $\omega_n = 2\pi T(n + \frac{1}{2})$ are the fermionic Matsubara frequencies, $\Delta_{\mathbf{k}}$ is the gap parameter at wave vector \mathbf{k} , N_0 is the two-spin density of states, $V_{\mathbf{k}, \mathbf{k}'}$ is the pairing interaction, $\langle \dots \rangle_{\text{FS}}$ denotes an average over the Fermi surface and ω_0 is a high frequency cutoff.

The two-band superconductor describes situations in which the gap variation over the Fermi surface is approximately bimodal and can be approximated by two distinct gap scales, Δ_1 and Δ_2 , one for each band. As discussed in Ref. [22], the Fermi surface average is replaced by a sum over bands, and the pairing interaction is parameterized by a 2×2 symmetric matrix $\lambda_{\mu\nu}$, with the diagonal terms λ_{11} and λ_{22} describing intraband pairing, and the off-diagonal terms $\lambda_{12} = \lambda_{21}$ the interband interaction. The gap equation then takes the simplified form

$$\Delta_\nu = \sum_{\mu=1,2} n_\mu \lambda_{\nu\mu} 2\pi T \sum_{\omega_n > 0}^{\omega_0} \frac{\Delta_\mu}{\sqrt{\Delta_\mu^2 + \hbar^2 \omega_n^2}}, \quad (5)$$

where the relative densities of states for each band, n_μ , obey $n_1 + n_2 = 1$. For a given choice of parameters $\{n_1, \lambda_{11}, \lambda_{22}, \lambda_{12}\}$, Eq. (5) is solved numerically, from which we obtain the temperature dependence of the gap parameters Δ_1 and Δ_2 , as shown, for example, in Fig. 5.

B. Superfluid Density

Superfluid density is a thermal equilibrium property of the superconductor and is readily obtained within the Matsubara formalism once the energy gaps are known. For band ν , the normalized superfluid density is

$$\rho_\nu(T) = \frac{\lambda_\nu^2(0)}{\lambda_\nu^2(T)} = \sum_{\omega_n > 0} \frac{\Delta_\nu^2}{(\Delta_\nu^2 + \hbar^2 \omega_n^2)^{3/2}}. \quad (6)$$

The total normalized superfluid density is a weighted sum of the contributions from each band,

$$\rho(T) = \gamma \rho_1(T) + (1 - \gamma) \rho_2(T), \quad (7)$$

where the weighting factor $0 < \gamma < 1$ is determined by the plasma frequency imbalance balance the bands. Note that γ is distinct from the density of states parameter n_1 , as it includes Fermi velocity information:

$$\gamma = \frac{n_1 v_1^2}{n_1 v_1^2 + n_2 v_2^2}, \quad (8)$$

where v_1 and v_2 are the rms Fermi velocities of the two bands.

C. Fitting procedure and results

A least-squares optimization is used to search for best-fit parameters in the four-dimensional parameter space $\{n_1, \lambda_{11}, \lambda_{22}, \lambda_{12}\}$. For each parameter choice, the band-specific energy gaps and superfluid densities are determined at each of the experimental temperatures via numerical solution of Eqs. (5) and (6). As shown in Eq. (7), the total superfluid density is a weighted combination of the band-specific superfluid densities. While the weighting coefficient γ is formally an additional fit parameter, a closed-form expression exists for its optimal value, so that it need not be included in the minimization search. γ_{opt} is found by minimizing the χ^2 merit function

$$\begin{aligned}\chi^2 &= \left| \frac{\vec{\rho}_{\text{expt}} - \vec{\rho}_{\text{model}}}{\vec{\sigma}} \right|^2 \\ &= \left| \frac{\vec{\rho}_{\text{expt}} - \vec{\rho}_2 - \gamma \Delta \vec{\rho}}{\vec{\sigma}} \right|^2 \\ &= \frac{\gamma^2 |\Delta \vec{\rho}|^2 - 2\gamma \Delta \vec{\rho} \cdot (\vec{\rho}_{\text{expt}} - \vec{\rho}_2) + |\vec{\rho}_{\text{expt}} - \vec{\rho}_2|^2}{|\vec{\sigma}|^2}\end{aligned}\quad (9)$$

where $\Delta \vec{\rho} = \vec{\rho}_1 - \vec{\rho}_2$. Here the vector quantities encode the discrete temperature dependences of the various quantities, including experimental and model superfluid densities, and the measurement errors $\vec{\sigma}$. Minimizing with respect to γ we obtain

$$\gamma_{\text{opt}} = \frac{\Delta \vec{\rho} \cdot (\vec{\rho}_{\text{expt}} - \vec{\rho}_2)}{|\Delta \vec{\rho}|^2}. \quad (10)$$

fit parameter	$n_1 = 0.8$	uncertainty	$n_1 = 0.9$	uncertainty
λ_{11}	0.27	± 0.013	0.84	± 0.063
λ_{22}	-0.14	± 0.0062	-0.37	± 0.0077
λ_{12}	1.62	± 0.11	1.98	± 0.083
γ_{opt}	0.69		0.49	

TABLE I. Best-fit parameters and their uncertainties, for $n_1 = 0.8$ and $n_1 = 0.9$.

In practice, the optimization depends only weakly on the choice of density of states parameter n_1 , which we set to fixed values. We present results in Table 1 for $n_1 = 0.8$ and $n_1 = 0.9$, noting that fits are noticeably worse for $n_1 < 0.8$ and $n_1 > 0.9$. Figures 2 and 5 show the fits and gaps for $n_1 = 0.8$, which are practically indistinguishable from the fits for $n_1 = 0.9$. Note that while the λ_{22} parameter appears to vary strongly between the two cases, it is the combination $n_2 \lambda_{22}$ that determines the intraband pairing strength in the second band, and this combination remains approximately constant. From this we conclude that the intrinsic pairing strength in the subdominant band is actually repulsive, and that LaNiGa₂ has a very significant interband contribution to its pairing. We reiterate that the experimental signature of this is the enhancement of $\rho_s(T)$ in the upper half of the superconducting temperature range, well in excess of the single-band BCS behaviour. We note that this is quite different from LaNiC₂, which shows no such enhancement, and has far less significant interband pairing.

ACKNOWLEDGMENTS

We thank the personnel of the Centre for Molecular and Materials Science at TRIUMF for technical assistance with our μ SR measurements. J.E.S. and S.R.D. acknowledge support from the Natural Sciences and Engineering Research Council of Canada (PIN: 146772). S.S. acknowledges support from the Engineering and Physical Sciences Research Council (EPSRC) through grant EP/P024564/1. The sample synthesis at UC Davis was supported by the UC Laboratory Fees Research Program (LFR-20-653926). H.B. was supported by the NSF-REU program PHY-2150515.

-
- [1] S. Das Sarma, M. Freedman, and C. Nayak, Majorana Zero Modes and Topological Quantum Computation, npj Quantum Information **1**, 15001 (2015).
 - [2] M. Sato, and Y. Ando, Topological superconductors: a review, Rep. Prog. Phys. **80**, 076501 (2017).
 - [3] J. R. Badger, Y. Quan, M. C. Staab, S. Sumita, A. Rossi, K. P. Devlin, K. Neubauer, D. S. Shulman, J. C. Fetting, P. Klavins, S. M. Kauzlarich, D. Aoki, I. M. Vishik, W. E. Pickett, and V. Taufour, Dirac lines and loop at the Fermi level in the time-reversal symmetry breaking superconductor LaNiGa₂, Commun. Phys. **5**, 22 (2022).
 - [4] A. D. Hillier, J. Quintanilla, B. Mazidian, J. F. Annett, and R. Cywinski, Nonunitary Triplet Pairing in the Centrosymmetric Superconductor LaNiGa₂, Phys. Rev. Lett. **109**, 097001 (2012).
 - [5] Z. F. Weng, J. L. Zhang, M. Smidman, T. Shang, J. Quintanilla, J. F. Annett, M. Nicklas, G. M. Pang, L. Jiao, W. B. Jiang, Y. Chen, F. Steglich, and H. Q. Yuan, Two-Gap Superconductivity in LaNiGa₂ with Nonunitary Triplet Pairing and Even Parity Gap Symmetry, Phys. Rev. Lett. **117**, 027001 (2016).
 - [6] G. Csire, B. Újfalussy, J. F. Annett, Eur. Phys. J. B **91**, 217 (2018).
 - [7] S. K. Ghosh, G. Csire, P. Whittlesea, J. F. Annett, M. Gradhand, B. Újfalussy, and J. Quintanilla, Quantitative theory of triplet pairing in the unconventional superconductor LaNiGa₂, Phys. Rev. B **101**, 100506(R) (2020).

- [8] A. D. Hillier, J. Quintanilla, and R. Cywinski, Evidence for Time-Reversal Symmetry Breaking in the Noncentrosymmetric Superconductor LaNiC_2 , *Phys. Rev. Lett.* **102**, 117007 (2009).
- [9] Shyam Sundar, S. R. Dunsiger, S. Gheidi, K. S. Akella, A. M. Côté *et al.*, Two-gap time reversal symmetry breaking superconductivity in noncentrosymmetric LaNiC_2 , *Phys. Rev. B* **103**, 014511 (2021).
- [10] W. H. Lee, H. K. Zeng, Y. D. Yao, and Y. Y. Chen, *Physica C* **266**, 138 (1996).
- [11] V. K. Pecharsky, L. L. Miller, and K. A. Gschneidner, Jr., Low-temperature behavior of two ternary lanthanide nickel carbides: Superconducting LaNiC_2 and magnetic CeNiC_2 , *Phys. Rev. B* **58**, 497 (1998).
- [12] Y. Iwamoto, Y. Iwasaki, K. Ueda, and T. Kohara, *Phys. Lett. A* **250**, 439 (1998).
- [13] S. Katano, K. Shibata, K. Nakashima, and Y. Matsubara, Magnetic impurity effects on the superconductivity of noncentrosymmetric LaNiC_2 : Ce substitution for La, *Phys. Rev. B* **95**, 144502 (2017).
- [14] J. Chen, L. Jiao, J. L. Zhang, Y. Chen, L. Yang, M. Nicklas, F. Steglich, and H. Q. Yuan, Evidence for two-gap superconductivity in the non-centrosymmetric compound LaNiC_2 , *New. J. Phys.* **15**, 053005 (2013).
- [15] I. Bonalde, R. L. Ribeiro, K. J. Syu, H. H. Sung, and W. H. Lee, Nodal gap structure in the noncentrosymmetric superconductor LaNiC_2 from magnetic-penetration-depth measurements, *New. J. Phys.* **13**, 123022 (2011).
- [16] J. F. Landaeta, D. Subero, P. Machado, F. Honda, and I. Bonalde, Unconventional superconductivity and an ambient-pressure magnetic quantum critical point in single-crystal LaNiC_2 , *Phys. Rev. B* **96**, 174515 (2017).
- [17] J. E. Sonier, J. H. Brewer and R. F. Kiefl, μSR studies of the vortex state in type-II superconductors, *Rev. Mod. Phys.* **72**, 769 (2000).
- [18] J. E. Sonier, F. D. Callaghan, R. I. Miller, E. Boaknin, L. Taillefer, R. F. Kiefl, J. H. Brewer, K. F. Poon, and J. D. Brewer, Shrinking Magnetic Vortices in V_3Si due to Delocalized Quasiparticle Core States: Confirmation of the Microscopic Theory for Interacting Vortices, *Phys. Rev. Lett.* **93**, 017002 (2004).
- [19] J. E. Sonier, Muon spin rotation studies of electronic excitations and magnetism in the vortex cores of superconductors, *Rep. Prog. Phys.* **70**, 1717 (2007).
- [20] K. Takanaka, Flux-Line Lattices of pure Type II Superconductors with Anisotropic Fermi Surface, *Prog. Theor. Phys.* **46**, 1301-1306 (1971).
- [21] J. Bardeen, L. N. Cooper, and J. R. Schrieffer, Microscopic Theory of Superconductivity, *Phys. Rev.* **106**, 162 (1957).
- [22] V. G. Kogan, C. Martin, and R. Prozorov, Superfluid density and specific heat within a self-consistent scheme for a two-band superconductor. *Phys. Rev. B* **80**, 014507 (2009).
- [23] R. Kadono, Field-induced quasiparticle excitations in novel type II superconductors, *J. Phys.: Condens. Matter* **16** S4421 (2004).
- [24] K. Ohishi, K. Kahuta, J. Akimitsu, W. Higemoto, R. Kadono, J.E. Sonier, A.N. Price, R.I. Miller, R.F. Kiefl, M. Nohara, H. Suzuki, and H. Takagi, Nonlocal effects and shrinkage of the vortex core radius in $\text{YNi}_2\text{B}_2\text{C}$ probed by muon spin rotation, *Phys. Rev. B* **65**, 140505(R) (2002).
- [25] A.N. Price, R.I. Miller, R.F. Kiefl, J.A. Chakhalian, S.R. Dunsiger, G.D. Morris, J.E. Sonier, and P.C. Canfield, Anomalous vortex state of superconducting $\text{LuNi}_2\text{B}_2\text{C}$, *Phys. Rev. B* **65**, 214520 (2002).
- [26] F. D. Callaghan, M. Laulajainen, C. V. Kaiser, and J. E. Sonier, Field Dependence of the Vortex Core Size in a Multiband Superconductor, *Phys. Rev. Lett.* **95**, 197001 (2005).
- [27] T. J. Williams, A. A. Aczel, E. Baggio-Saitovitch, S. L. Bud'ko, P. C. Canfield, J. P. Carlo, T. Goko, J. Munevar, N. Ni, Y. J. Uemura, W. Yu, and G. M. Luke, Muon spin rotation measurement of the magnetic field penetration depth in $\text{Ba}(\text{Fe}_{0.926}\text{Co}_{0.074})_2\text{As}_2$: Evidence for multiple superconducting gaps, *Phys. Rev. B* **80**, 094001 (2009).
- [28] S. Weyeneth, M. Bendele, R. Puzniak, F. Murányi, A. Bussmann-Holder, N. D. Zhigadlo, S. Katrych, Z. Bukowski, J. Karpinski, A. Shengelaya, Field-dependent superfluid density in the optimally doped $\text{SmFeAsO}_{1-x}\text{F}_y$ superconductor, *Europhys. Lett.* **91**, 47005 (2010).
- [29] Rustem Khasanov, Hubertus Luetkens, Alex Amato, Hans-Henning Klauss, Zhi-An Ren, Jie Yang, Wei Lu, and Zhong-Xian Zhao, Muon spin rotation studies of $\text{SmFeAsO}_{0.85}$ and $\text{NdFeAsO}_{0.85}$ superconductors, *Phys. Rev. B* **78**, 092506 (2008).
- [30] R. Khasanov, A. Shengelaya, A. Maisuradze, F. La Matina, A. Bussmann-Holder, H. Keller, and K. A. Müller, Experimental Evidence for Two Gaps in the High-Temperature $\text{La}_{1.83}\text{Sr}_{0.17}\text{CuO}_4$ Superconductor, *Phys. Rev. Lett.* **98**, 057007 (2007).
- [31] S. Serventi, G. Allodi, R. De Renzi, G. Guidi, and L. Romanò, P. Manfrinetti, A. Palenzona, Ch. Niedermayer, A. Amato, and Ch. Baines, Effect of Two Gaps on the Flux-Lattice Internal Field Distribution: Evidence of Two Length Scales in $\text{Mg}_{1-x}\text{Al}_x\text{B}_2$ from μSR , *Phys. Rev. Lett.* **93**, 217003 (2004).
- [32] H. Luetkens, H.-H. Klauss, R. Khasanov, A. Amato, R. Klingeler, I. Hellmann, N. Leps, A. Kondrat, C. Hess, A. Köhler, G. Behr, J. Werner, and B. Büchner, Field and Temperature Dependence of the Superfluid Density in $\text{LaFeAsO}_{1-x}\text{F}_x$ Superconductors: A Muon Spin Relaxation Study, *Phys. Rev. Lett.* **101**, 097009 (2008).
- [33] Kyuil Cho, M. Kończykowski, S. Ghimire, M. A. Tanatar, Lin-Lin Wang, V. G. Kogan, and R. Prozorov, Multi-band $s++$ superconductivity in V_3Si determined from the response to a controlled disorder, *Phys. Rev. B* **105**, 024506 (2022).
- [34] S. Ding, D. Zhao, T. Jiang, H. Wang, D. Feng, and T. Zhang, Surface structure and multigap superconductivity of V_3Si (111) revealed by scanning tunneling microscopy, *Quantum Frontiers* **2**, 3 (2023).
- [35] J. E. Sonier, R. F. Kiefl, J. H. Brewer, J. Chakhalian, S. R. Dunsiger, W. A. MacFarlane, R. I. Miller, A. Wong, G. M. Luke, and J. W. Brill, Muon-Spin Rotation Measurements of the Magnetic Field Dependence of the Vortex-Core Radius and Magnetic Penetration Depth in NbSe_2 , *Phys. Rev. Lett.* **79**, 1742 (1997).
- [36] M. Ichioka, A. Hasegawa, and K. Machida, Vortex lattice effects on low-energy excitations in d -wave and s -wave superconductors, *Phys. Rev. B* **59**, 184 (1999).
- [37] M. Ichioka, A. Hasegawa, and K. Machida, Field dependence of the vortex structure in d -wave and s -wave superconductors, *Phys. Rev. B* **59**, 8902 (1999).
- [38] E. Boaknin, M. A. Tanatar, J. Paglione, D. Hawthorn, F. Ronning, R. W. Hill, M. Sutherland, L. Taillefer, J.

- Sonier, S. M. Hayden, and J. W. Brill, Heat Conduction in the Vortex State of NbSe₂: Evidence for Multiband Superconductivity, Phys. Rev. Lett. **90**, 117003 (2003).
- [39] V. G. Kogan and N. V. Zhelezina, Field dependence of the vortex core size, Phys. Rev. B **71**, 134505 (2005).
- [40] M. Ichioka, V. G. Kogan, and J. Schmalian, Locking of length scales in two-band superconductors, Phys. Rev. B **95**, 064512 (2017).
- [41] A. Vargunin and M. A. Silaev, Field dependence of the vortex-core size in dirty two-band superconductors, Phys. Rev. B **100**, 014516 (2019).